Columbia International Publishing
Advances in Alloys and Compounds
(2014) Vol. 1 No. 2 pp. 46-53

Research Article

Tuning the Corrosion Behavior of Rapidly Solidified and Thermally-annealed Fe-Ti-Pd Alloys

Sergio Gonzalez[1*] and Jordi Sort[2]

Received 10 April 2014; Published online 14 June 2014

Abstract

The corrosion behavior of rapidly solidified $Fe_{(91-x)}Ti_9Pd_x$ (x=0, 1, 3 5) alloys (wt. %), both in the as-cast and thermally annealed (i.e., slowly cooled) states, has been investigated by means of electrochemical potentiodynamic polarization and immersion tests. Addition of Pd shifts the corrosion potential towards more anodic values than in the $Fe_{91}Ti_9$ alloy, both in the as-cast and annealed samples. In turn, the processing route (rapid cooling vs. thermal annealing) has a strong influence in the resulting microstructure, thus inducing drastic changes in the corrosion resistance. The values of corrosion potential in the as-cast samples increase with the Pd content since the cooling rate during casting is fast enough to allow Pd entering the Fe-Ti solid solution, hence making the alloy overall nobler. Conversely, the resistance against corrosion becomes lower in the heat-treated samples, presumably due to the precipitation of noble Pd-rich phases, which promote formation of micro-galvanic pairs.

Keywords: Fe-based alloy; Corrosion; Palladium; Heat treatment

1. Introduction

Fe-based alloys are used in a wide variety of industrial applications (e.g., machinery, magnetic, construction, etc.) due to their interesting properties, such as high strength and excellent machinability. However, these alloys exhibit poor corrosion resistance in water environments, especially in salt-containing water. Fe-based alloys are also interesting for implant applications due to their biocompatibility and relatively low cost. However, the biocompatibility of Fe is smaller than that of other elements (e.g., Ti) and the Young's modulus is much higher than that of bone. Partly substituting Fe by Ti allows improving the biocompatibility and decreasing the Young's modulus, while increasing the wear and corrosion resistance, thus minimizing the release of wear debris and ions into the body.

*Corresponding e-mail: Sergio.Gonzalez@uab.cat
1* Departament de Física, Facultat de Ciències, Universitat Autònoma de Barcelona, E-08193 Bellaterra, Spain
2 Institució Catalana de Recerca i Estudis Avançats (ICREA) and Departament de Física, Universitat Autònoma de Barcelona, E-08193 Bellaterra, Spain

To control the corrosion rate of a metal, different approaches can be followed. These include alloying (Liu and Zheng, 2011) or controlling the microstructure through metal forming (Moravej et al., 2010). Previous works on the improvement of corrosion of Fe base alloys with alloying elements is scarce and basically focused on amorphous Fe-P-C alloy (Hashimoto et al., 1979) and stainless steel (Hermas et al., 1995). Alloying with a small amount of Pd, a more noble element than Fe and Ti, should normally increase the corrosion resistance of Fe-Ti, provided that a homogeneous microstructure is preserved (i.e., if Pd enters the existing phases forming solid solutions). However, if precipitation of Pd-rich particles occurs, then these precipitates can act as cathodic sites that induce micro-galvanic corrosion (Schinhammer et al., 2010; Pellicer et al., 2013) and thus accelerate the corrosion rate.

The aim of this work is to investigate to what extent it is possible to improve the corrosion resistance of rapidly solidified $Fe_{91}Ti_9$ through addition of small amounts of Pd while minimizing formation of Pd-rich precipitates, which are detrimental in terms of corrosion resistance. To ascertain the importance of adequate tailoring of the alloy microstructure in the corrosion behavior, the as-cast samples have been also annealed and the resulting corrosion performance has been correlated with the observed microstructural changes. The $Fe_{91}Ti_9$ (wt. %) composition was selected since the amount of Ti is close to the solubility limit for Ti in -Fe (around 8.4 wt. %) (Okamoto, 2000). The ability to tune the corrosion behavior of this alloy through Pd addition is appealing its use in widespread engineering applications, such as in the biomedical field.

2. Experimental

Master alloys with composition $Fe_{(91-x)}Ti_9Pd_x$ (x=0, 1, 3 5) (labelled as Fe-9Ti, Pd1, Pd3 and Pd5, respectively) were prepared by arc melting a mixture of the pure elements (> 99.9 at. %) in a Ti-gettered high purity argon atmosphere. The master alloys were remelted at least three times to get chemically homogeneous ingots. Rod samples of 2 mm in diameter were obtained from the melt by injecting the master alloy into a copper mould in an inert gas atmosphere. The structure of the as-cast samples was studied by X-ray diffraction (XRD) (Philips X'Pert) with monochromated Cu Kα radiation (30º-75º 2θ range, counting time: 7 s, step size: 0.02º). The microstructure was observed with a scanning electron microscope (SEM) (Zeiss EVO) equipped with energy dispersive X-ray (EDX) analysis. The alloys containing 1, 3 and 5 wt. % Pd were thermally treated at 500ºC for 10 h (heat treatment HT1) to favour precipitation of Pd-containing phases. The alloy containing 5 wt. % Pd was additionally heat treated at 1100ºC for 30 min + 600ºC for 10 h (heat treatment HT2) to further favour formation of Pd-rich precipitates.

The corrosion behaviour was studied qualitatively by potentiodynamic polarization tests in Hank's solution (simulated body fluid, SBF, purchased from Aldrich) at 310 K and 1mV/s. The electrochemical experiments were performed in a thermostatized, one-compartment three-electrode cell. A double junction Ag|AgCl reference electrode was used with 3 M KCl inner solution and 1 M NaCl outer solution. A Pt sheet acted as a counter electrode. To evaluate the time-dependence of metal ions released from the samples, disk samples were introduced into sterilized plastic containers filled with Hank's solution. Afterwards, the containers were sealed and placed into a thermostatized bath at 37ºC. After 3 days and 10 days aliquots of Hank´s solution were

pipette off and analyzed by inductively coupled plasma-optical emission spectroscopy (ICP-CM). Surface topology measurements were carried out using a Leica DCM 3D profilometer.

3. Results and Discussion

Fig. 1 shows the XRD scans of the as-cast (i.e., rapidly cooled) (Fig. 1a) and heat treated (Fig. 1b) samples for all the compositions. The peaks have been identified and indexed using the JCPDS International Centre Database. In the as-cast condition, high intensity (110), (200) and (211) peaks associated to bcc cubic Im3m α-Fe have been detected in all the composition (Cui, 2008). For the alloy containing 3 wt. % Pd, small intensity peaks associated to tetragonal I4/mmm $TiPd_2$ (a=b=0.324, c=0.848 nm) are also detected. Finally, for the alloy with 5 wt. % Pd, low intensity peaks corresponding to $TiPd_2$ and to hexagonal $P6_3/mmc$ $TiPd_3$ (a=b=0.54917 nm and c=0.89692 nm) are present. The formation of Ti-Pd intermetallic richer in Pd as Pd is increasingly added to the alloy, is consistent with what should be expected from the binary Fe-Ti diagram and the nominal composition of the alloy. After the heat treatments, the peaks corresponding to $TiPd_2$ and $TiPd_3$ increase in intensity. These results are consistent with the binary Ti-Pd diagram since in order to have a Ti-rich eutectic region, the α-Fe grains have to be depleted in Ti to balance the nominal composition.

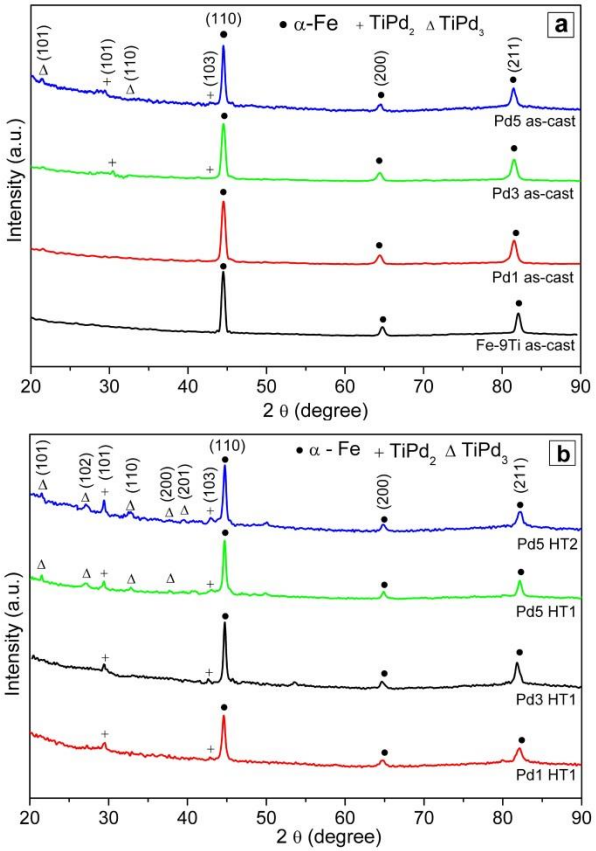

Fig. 1. XRD patterns of (a) as-cast Fe-9Ti, Fe-9Ti-1Pd, Fe-9Ti-3Pd and Fe-9Ti-5Pd alloys and (b) heat treated Fe-9Ti-1Pd, Fe-9Ti-3Pd and Fe-9Ti-5Pd alloys.

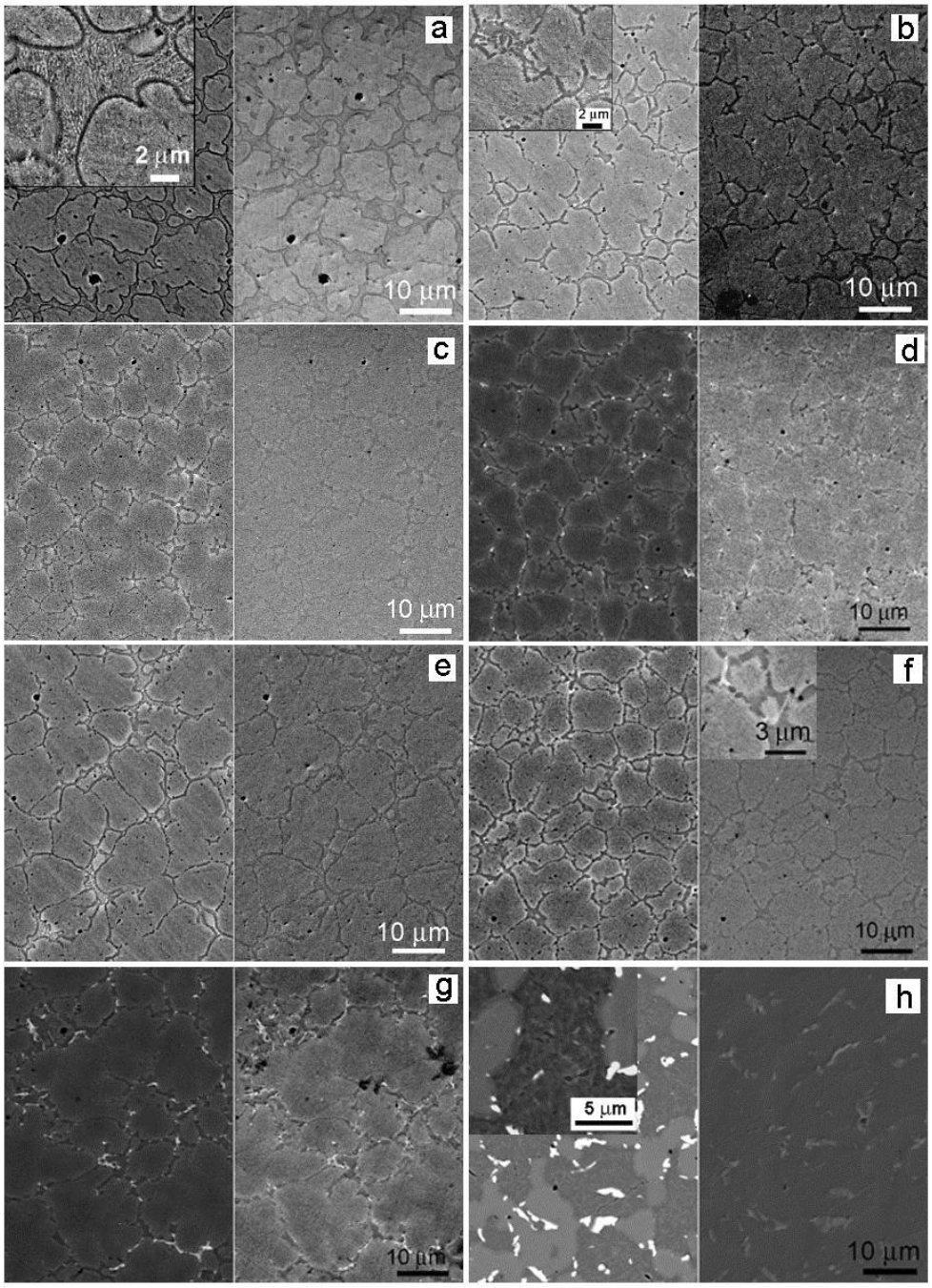

Fig. 2. SEM images of as-cast (a) Fe-9Ti, (b) Fe-9Ti-1Pd, (c) as-cast Fe-9Ti-3Pd, (d) as-cast Fe-9Ti-5Pd, (e) Fe-9Ti-1Pd HT T1, (f) Fe-9Ti-3Pd HT T1, (g) Fe-9Ti-5Pd HT T1, (h) Fe-9Ti-5Pd HT T2. Note that the right and left panels correspond to secondary and backscattered electrons images, respectively.

Fig. 2 shows the microstructures of the as-cast and heat treated samples for all the compositions. To better compare the microstructural differences, not only the secondary (right) but also the

backscattered (left) SEM images are presented. The microstructure of the Fe-9Ti (Fig. 2a) alloy consists of grains of about 10 μm size and grain boundaries containing a fine eutectic microstructure (inset: backscattered image). The composition of the grains is about $Fe_{92.4}Ti_{7.6}$ (wt. %) i.e., larger Ti content in solid solution than in equilibrium condition at room temperature [8] but smaller than the nominal composition. This behavior is due to the rapid solidification process, which is fast enough to retain elements in solid solution that otherwise would tend to segregate and form precipitates. The general composition of the eutectic region is richer in Ti (from 15.5 to 16.3 wt. % Ti) than the nominal composition although the exact composition of each phase within the eutectic could not be accurately measured due to their small size.

The backscattered electrons SEM image of the alloy with 1 wt. % Pd (Fig. 2b) shows that the brightness of the grains is not homogeneous. Lighter contrast is observed close to the grain boundary, suggesting enrichment in an element with high atomic weight, presumably Pd (see magnified backscattered image of inset). This indicates that the cooling rate during the sample fabrication was not high enough to avoid partial segregation of Pd from inside the grains. The content of Ti in solid solution within the α-Fe grains (7.6-8 wt. %) is practically the same as for the Fe-9Ti alloy. The Pd content inside the grains (0.9 wt. %) is lower than the nominal composition, but the opposite is observed at the grain boundaries (Pd content around 1.5-2 wt. %)

Larger addition of Pd (3 wt. %) leads to the formation of Pd-rich precipitates of about 2 μm size at the grain boundaries (Fig. 2c) although most of Pd (~2.5 wt. %) still remains in solid solution inside the α-Fe grains. For the alloy with 5 wt. % Pd (Fig. 2d) the concentration of Pd in solid solution is larger than for the Pd3 alloy although the precipitates are also slightly larger (~ 4μm). This suggests that the concentration of Pd is close to the limit to be totally retained in solid solution and starts to segregate in larger amounts.

The segregation of Pd is promoted by subsequent thermal treatment (Figs. 2e, f, g and h). This precipitation is evidenced from the higher contrast of the grain boundaries. For Pd1 (backscattered image of Fig. 2e) and Pd3 (backscattered image of Fig. 2f) alloys, the HT1 heat treatment practically does not coarsen the precipitates but leads to an increase in volume fraction in Pd-rich precipitates. The precipitates of the Pd5 alloy grow further after heat treatment to HT1 conditions (Fig. 2g), leading to the formation of a nearly continuous network of precipitates. These precipitates become more round-shaped and larger (of about 8 μm) after annealing using HT2 conditions (Fig. 2h). These observations are in agreement with the results obtained from XRD (Fig. 1b). However, annealing does not have an important effect on the grain size, i.e., the differences are within the dispersion error, as can be deduced from the SEM images and from the similar width of the XRD peaks corresponding to α-Fe.

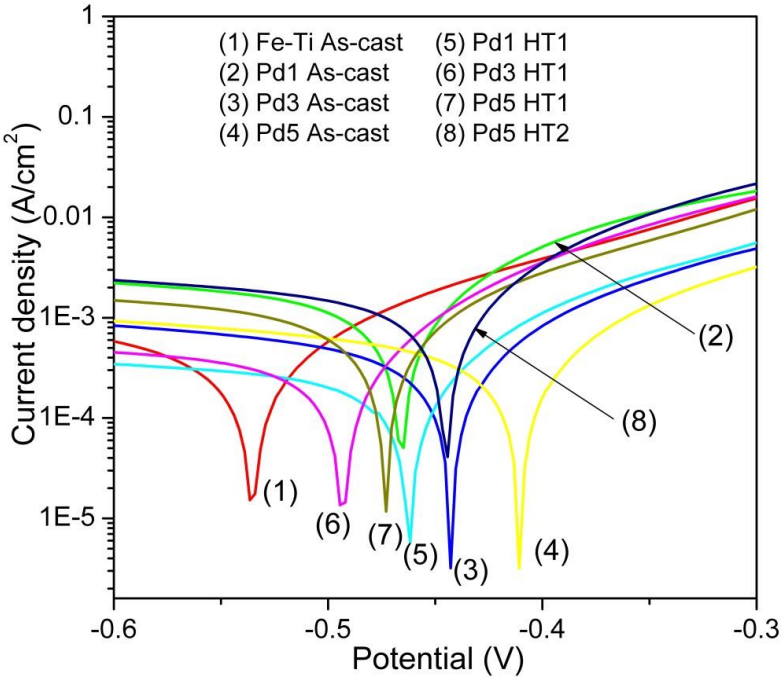

Fig. 3. Potentiodynamic polarization curves for the as-cast and heat treated compositions.

Fig. 3 shows the potentiodynamic polarization curves of the $Fe_{(91-x)}Ti_9Pd_x$ (x=0, 1, 3 5) (wt. %) alloys in the as-cast condition and after being heat treated. For the as-cast samples, the increase in the amount of Pd shifts the corrosion potential (E_{corr}) towards more anodic values, from -0.5365 V for Fe-9Ti to -0.4108 V for the Pd5 alloy, indicating that the addition of Pd delays the onset of corrosion. Subsequent heat treatments tend to decrease E_{corr} towards more cathodic values. In this case, corrosion is accelerated due to the formation of micro-galvanic pairs caused by the precipitation of Pd-rich phases (Fig. 2). Specifically, heat treatment of the Pd1 alloy in HT1 conditions does not significantly shift E_{corr}, which is consistent with the slight microstructural changes occurring upon annealing. However, E_{corr} of the as-cast Pd3 and Pd5 alloys shift by about -0.0516 and -0.0621 V, respectively, after HT1 heat treatment since the content of Pd is high enough to promote precipitation of Pd-rich particles. However, heat treating the Pd5 alloy at HT2 conditions does not further decrease E_{corr} towards more cathodic values but towards more anodic values. This suggests that since Pd-rich precipitates become coarser after annealing at HT2, the number of galvanic pairs may become effectively smaller than after annealing at HT1, thus resulting in an improvement of the corrosion resistance. The lowest E_{corr} and thus the maximum expected susceptibility to corrosion is attained by the Pd3 alloy heat treated at HT1 conditions for which the microstructure consists of Pd-rich particles of up to 3 micron size (Fig. 2f).

To study in more detail which of the alloys with the lowest E_{corr} values is more sensitive to corrosion and also to tackle the influence of heat treatments on the corrosion behavior, the as-cast Fe-9Ti alloy and the Pd3 and Pd5 heat treated alloys were immersion tested into Hank´s solution for 3 and 10 days (Fig. 4a and 4b). The concentration, i.e., mass loss, and calculated corrosion rate of Fe released into the solution as a function of immersion time was recorded. The loss of Ti or Pd during immersion was negligible. The loss of Fe is fast for short immersion times, i.e., maximum

corrosion rate is attained after 3 h, but it slows down for longer times. For the Pd3 alloy heat treated at HT1 conditions, the mass loss was 132 and 174 μg^{-1} after 3 and 10 days, respectively, higher than the mass loss of the Fe-9Ti and Pd5 alloy. Fig. 4b shows that the degradation rate decreases with increasing immersion time. This behavior is especially noticeable for the Pd3 alloy heat treated at HT1 conditions. The slower release of Fe from the heat treated Pd5 alloy than from the heat treated Pd3 alloy is consistent with the potentiodynamic polarization curves. However, although the concentration of Fe released is smaller for the Fe-9Ti alloy than for the heat treated Pd3 alloy, the E_{corr} of the former alloy is smaller. This behavior can be explained considering that the potentiodynamic tests give information about the corrosion kinetics while the immersion tests provide information about evolution of the degradation. These results thus suggest that although the corrosion behavior of the Fe-9Ti alloy starts earlier, the Pd3 alloy corrodes faster for longer immersion times. Similar observations have been reported in Mg-based metallic glasses after addition of different Pd percentages (Pellicer et al., 2013). Considering the similar grain size and morphology (dendritic) of the grains, we can conclude that the difference in corrosion performance is mainly due to the differences in composition, i.e., elements in solid solution, and precipitates size and morphology.

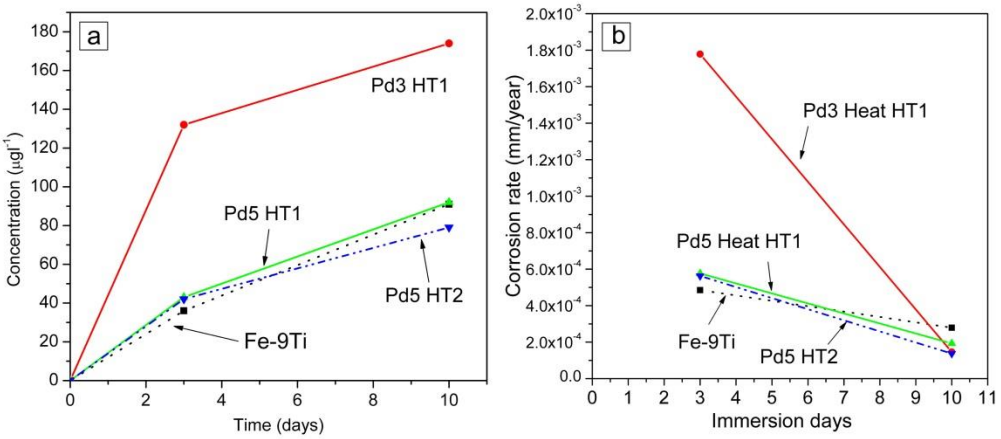

Fig. 4. (a) Concentration of Fe in the Hank´s solution and (b) corrosion rate over different immersion times for the as-cat and heat treated compositions.

Finally, the average surface roughness (S_a) for some samples immersed in SBF at 37ºC for 10 days was measured by profilometry (Table 1).The minimum S_a value was attained in the Pd5 alloy heat treated at HT2 conditions (0.089 μm), while S_a was maximum for the Pd3 heat treated in HT1 conditions (0.211 μm). Intermediate values were measured for Fe-9Ti (0.140 μm) and Pd5 HT1 (0.170 μm). This trend is consistent with the differences in corrosion behavior observed (Fig. 3) and confirms that the highest corrosion is attained by the Pd3 HT1 alloy.

Table 1 Profilometry results of the samples after immersion in SBF at 37ºC for 10 days.

Material	S_a(m)
Fe-9Ti	0.140
Pd3 HT1	0.211
Pd5 HT1	0.170
Pd5 HT2	0.089

4. Conclusions

1. This work reveals that rapid solidification is a suitable technique to obtain an appropriate microstructure that optimizes the corrosion resistance of Ti-Fe-Pd alloys.
2. Our results reveal the importance of the size and distribution of Pd-based precipitates on the corrosion performance of Fe-9Ti alloy.
3. The highest corrosion resistance is attained in the alloy with 5 wt. % Pd since the rapid solidification technique allows most of Pd atoms entering the Fe-Ti solid solution.
4. Heat treatments lead to the formation of Pd-rich precipitates which act as microgalvanic pairs that promote corrosion. The corrosion performance, however, depends on the size and distribution of the precipitates.
5. Among the compositions and heat treatments studied, maximum corrosion behavior is attained by the 3 wt. % Pd alloy treated at HT1 conditions whose microstructure consists of a continuous network of Pd-rich precipitates slightly smaller than 3 μm.

Acknowledgements

This work has been partially financed by the 2014-SGR-1015 and MAT2011-27380-C02-01 research projects. S.G. acknowledges the Juan de la Cierva Fellowship from the Spanish Ministry of Science and Innovation.

References

Hashimoto, K., Asami, K., Naka, M., Masumoto, T. (1979). The role of alloying elements in improving the corrosion resistance of amorphous iron base alloys. Corrosion Science, 19, 857-867. http://dx.doi.org/10.1016/S0010-938X(79)80080-3

Hermas, A.A., Ogura, K., Takagi, S., Adachi, T. (1995). Effects of alloying additions on corrosion and passivation behaviors of type 304 stainless steel. Corrosion Science, 51, 3-10. http://dx.doi.org/10.5006/1.3293575

Liu, B., & Zheng, Y.F. (2011). Effects of alloying elements (Mn, Co, Al, W, Sn, B, C and S) on biodegradability and in vitro biocompatibility of pure iron. Acta Biomat., 7, 1407-1420. http://dx.doi.org/10.1016/j.actbio.2010.11.001

Moravej, M., Purnama, A., Fiset. M., Couet, J., & Mantovani, D. (2010). Fe-Mn alloys for metallic biodegradable stents: Degradation and cell visibility studies. Acta Biomat., 6, 1843-1851. http://dx.doi.org/10.1016/j.actbio.2010.01.008

Okamoto H. Desk Handbook. Phase Diagrams for Binary Alloys. ASM International, Materials Park OH; 2000.

Pellicer, E., González, S., Blanquer, A., Suri-ach, S., Baró, M.D., Barrios, L., Ibá-ez, E., Nogués, C., & Sort, J. (2013). On the biodegradability, mechanical behavior and cytocompatibility of amorphous Mg72Zn23Ca5 and crystalline Mg70Zn23Ca5Pd2 alloys as temporary implant materials. J. Biomed. Mat. Research, Part A (101), 502-517

Schinhammer, M., Hänzi, A.C., Löffler, J.F., & Uggowitzer, P.J. (2010). Design strategy for biodegradable Fe-based alloys for medical applications. Acta Biomat., 6, 1705-1713. http://dx.doi.org/10.1016/j.actbio.2009.07.039